PCCP

Accepted Manuscript

ROYAL SOCIETY OF CHEMISTRY

www.rsc.org/pccp

Structure and energy level alignment at dye-electrode interface in p-type DSSC: new hints on the role of anchoring modes from *ab initio* calculations.

Ana B. Muñoz-García* and Michele Pavone*

Department of Chemical Sciences, University of Naples Federico II

Complesso Universitario Monte Sant'Angelo Via Cintia, 80126 Naples, Italy

* Corresponding authors:

A. B. Muñoz-García: anabelen.munozgarcia@unina.it - Tel: +39 081674202 - Fax: +39 081674330

M. Pavone: michele.pavone@unina.it - Tel: +39 081674210 - Fax: +39 081674330

Abstract

p-type dye-sensitized solar cells (DSSCs) represent the complementary photocathodes to the well-studied n-type DSSCs (Grätzel cells), but their low performances have hindered the development of convenient tandem solar cells based on cost-effective n- and p-type DSSCs. At the origin of the low efficiencies, experimental investigations highlighted the role of hole/electron transport processes at the dye-electrode interface. However, the effects of the dye anchoring groups on interfacial electronic features are still unclear. We report here a first principles study of a benchmark p-type DSSC model, namely the widely used Coumarin-based dye C343 adsorbed on p-NiO surface. Together with the original carboxylic acid, we test the alternative phosphonic acid as anchoring group. We investigate binding energies, structural features and electronic energy level alignments: our results highlight that these properties are highly sensitive to the binding modes. In particular, both the chemical nature of the anchoring group and the binding mode strongly affect the thermodynamic driving force for the dye-electrode hole injection process. From analysis of the electronic densities, we find that favorable driving forces are correlated to small values of the interfacial electrostatic dipole that is formed upon dye adsorption. From our results, we derive new hints for improving open circuit potential and hole injection process in p-type DSSCs based on NiO electrodes.

Keywords

Dye-sensitized solar cell; dye-electrode interface; dye anchoring groups; energy level alignment; DFT+U

Introduction

Sunlight is among the most convenient options for depleting fossil fuels as energy source: photovoltaic (PV) technologies target the efficient harvesting and conversion of solar energy into electricity.[1] Since the seminal work by O'Regan and Grätzel,[2] Dye-Sensitized Solar Cells (DSSCs) have attracted a great deal of interest as cost-effective alternative to solid-state PV solar panels. After two decades of intense research, DSSCs have achieved top efficiencies (electrical output versus incident solar energy) that exceed 12%.[3] The standard DSSC set up consists of a nano-heterogeneous photo-anode, made of n-type semiconductor (SC) nanoparticles (typically, TiO_2 or ZnO) sensitized with light-absorbing organic or metallo-organic dyes, an electrolyte solution and a metal as counter-electrode.[4] In the last years, Grätzel-like cells have seen an incredible boost in efficiency (up to ~20%) thanks to solid-state sensitizers made of an halogen metal-organic perovskite; these cells are very promising, but present major stability issues.[5] Another route to enhance DSSC efficiency is directed toward the development of tandem cells.[6] In these devices, a standard n-type DSSC is combined with a complementary p-type DSSC as photo-cathode so that the harvesting window increases, pushing forward the theoretical limit of photoconversion efficiency.[4,7] Unfortunately, the top efficiencies achieved so far for p-type DSSCs are lower than 2%.[8] This would wreck the overall performance of any possible tandem cell. Research on p-type DSSCs is indeed still in its infancy and lately, an increasing number of works are focusing on these devices.[9] In p-type DSSC, energy conversion takes place in a series of chained electronic processes, as depicted by **Scheme 1**: (1) excitation of the dye (D); (2) electron injection from the excited dye (D*) to the electrolyte and (3) electron injection from the p-type SC valence band (VB) to the HOMO of the dye (*i.e.*, hole transport from the dye to the p-SC VB). Undesired processes are (4) charge recombination at the dye-SC interface (D*-VB) and (5) hole injection from the dye (or from the p-SC VB) to the electrolyte.[10] The p-type DSSC low efficiencies reported so far have been ascribed to major limitations of current materials, regarding slow hole injection (3) and fast charge recombination (4) at the dye-electrode interface.[11]

Experimental progresses for p-type DSSCs have focused independently on the dye chemical structure,[12] the electronic features of p-type inorganic SCs [13] and the electrolyte redox couple.[14] However, improvements of a single component do not often translate to more effective devices. The inherent complexities of each constitutive element and interface have hindered the successful application of a combinatorial approach. Only a fundamental understanding of materials and interfaces structure-property-function relationships can enable a rational design of better performing p-type DSSCs. To this end, experimental investigations can strongly benefit of first-principles modeling approaches, following the successful examples of theoretical studies on n-type DSSCs.[15]

Only few first-principles studies have addressed p-type DSSCs, so far. Most report properties of isolated molecular sensitizer (in some cases the model accounts for the solvent),[16] or solid state p-SC materials.[17]

While several *ab initio* studies report the features of dye-electrode interface in n-type DSSCs,[15] there are no similar studies on the interfaces that are relevant to p-type DSSCs.

Here, we report the first *ab initio* study of a realistic model of a benchmark p-type DSSC system: the Coumarin-based C343 dye adsorbed on nickel oxide (NiO).[8-11,18] We investigated with density functional theory[19,20] (DFT)-based methods the structure, energetics and electronic properties of the NiO(100)/C343 interface, and how the interfacial features can tune some relevant parameters for p-type DSSC functioning.

Nickel oxide is certainly not the optimum p-SC for for p-type DSSC, because its VB edge position is too close to common electrolyte redox couple potentials, which results in low open circuit potentials (V_{OC}, see Scheme 1).[8,9,21] Nevertheless, some features have made NiO the reference material for tests and development of these devices:[4] it is inexpensive and relatively easy to manipulate, it presents an indirect band gap of ~3.6 eV with charge-transfer character and it has an intrinsic p-type SC nature due to the presence of nickel vacancies.[8,9,13,21]

In C343, the α-carbon to the carbonyl group of 2,3,5,6-1H,4H-tetra-hydroqunolizino[9,9A,1-GH] Coumarin (C6H) is functionalized with a carboxylic acid group (-CO_2H). As in n-type DSSCs, the vast majority of dyes used in p-type DSSCs feature this group as the anchoring moiety to the transition-metal surface.[4,8,9] However, the electronic features that makes -CO_2H efficient in n-type DSSCs (i.e., -CO_2H bearing high LUMO density) make it less suitable for p-type DSSCs because the strong overlap between the dye LUMO and p-SC valence band increases the probability of charge recombination. To prevent this process (arrow n. 4 in Scheme 1) the dye electronic structure plays a central role: the excited electronic state (LUMO) must be localized on the dye moiety that is furthest from the p-SC surface. For this reason, so-called *push-pull* dyes with intra-molecular charge-transfer upon photo-excitation have been developed so to have the HOMO density close to p-SC VB and the LUMO well exposed to the electrolyte solution.[13,14] While these features concerns only the dye, other desired features depend on the dye-electrode interface: the binding of the dye onto the p-SC surface should be strong and the absolute position of dye HOMO must be well below the p-SC VB edge, so to enhance the thermodynamic driving force for hole injection (ΔE in Scheme 1).[9] Current research browses other anchoring groups (phosphonic acid, bis-carbodithiolic acid, sulfonic acid, cathecol or acetyl acetonate groups, among others) in search for higher efficiencies.[22,23] To test the role of the anchoring group on dye-electrode interfacial properties, here we discuss both C343 and a model C6H Coumarin functionalized with the phosphonic acid group (-PO_3H_2). The two anchoring groups (-CO_2H and -PO_3H_2) can interact with the NiO surface with O atoms and/or OH groups, thus we also investigated the effects of the different possible binding modes on the Coumarin-NiO electronic structure.

From the analysis of our *ab initio* results, we derive new unbiased insights on the subtle structural and electronic features of the dye-electrode interface. In particular we highlight how the local structure at the interface can affect relevant parameters for p-type DSSC performance, such as the dye binding strength, the open circuit potential (V_{OC}) and the dye -> electrode hole injection driving force (ΔE).

Our study is not only relevant for p-DSSCs but also for analogous dye-sensitized photocatalytic systems, recently proposed in the context of artificial photosynthesis (*i.e.*, water splitting).[24] In these cells, the photo-exited dye transfer the electron onto a catalytic moiety (*e.g.*, a transition metal complex) that is co-adsorbed with the dye on the solid electrode. Hammström and co-workers have reported an efficient proton-reducing photo-electrochemical cell made of a p-type NiO electrode and the C343 dye with an Fe-based catalyst.[24] In such cell, after the electron transfer from the excited C343 and the catalyst, the hole injection from the dye to the p-NiO surface is a crucial step for dye regeneration and thus for enabling a new catalytic cycle.

Results and discussion

The two model dyes under study are α-functionalized derivatives of the C6H chromophore. Whether the substituent is the widely exploited carboxylic acid group (-CO_2H) or the recently proposed phosphonic acid group (-PO_3H_2), they are referred as CCO_2 and CPO_3 throughout the text, respectively. CCO_2 is the well known C343 dye. To the best of our knowledge, CPO_3 has not been tested experimentally, but this model dye allows us to factorize out the role of the anchoring group by direct comparison to the C343 case.

In order to evaluate to what extent the features of the two anchoring groups affect the properties of the dyes, we first analyzed the structural and electronic properties of isolated CCO_2 and CPO_3. Figure 1 depicts the optimized geometries, the calculated HOMO/LUMO distribution and the total density of states (DOS) of both dyes. The minimum energy structures and the HOMO/LUMO densities of the chromophore (i.e. the C6H moiety) are unaltered by changing the anchoring group. Also the DOS plots of both molecules present a very similar pattern and the HOMO-LUMO energy gap is not sensibly altered by the change in the anchoring group. However, the LUMO density localized on the anchoring group is lower in CPO_3 than in CCO_2. A lower LUMO density on the anchoring moiety implies weaker overlap between the dye LUMO and the p-SC VB. Since this overlap is responsible for the unwanted charge recombination process after dye photoexcitation, -PO_3H_2 group is, in principle, a better anchoring group for p-DSSCs than -CO_2H.

By preserving or losing acidic H from of -CO_2H and –PO_3H_2, CCO_2 and CPO_3 dyes can bind to NiO(100) surface in different configurations or *binding modes*: mono-dentate (M), bi-dentate (B) and - only for CPO_3 - tri-dentate (T), as depicted by Figure 2. Protons leaving the anchoring groups in the B and T modes are left to relax onto surface oxygen atoms and form protruding OH groups, which distort the surface. We tested all possible sites for surface OH formation and we fond that the energetic and electronic properties are independent to the final position of the leaving protons. Table 1 lists the main structural features ($O/H_{(dye)}$-$Ni/O_{(NiO)}$ distances and surface RMSD) for each relaxed dye-NiO system, together with the corresponding adsorption energy ($E_{ads} = E_{dye/NiO(100)} - E_{dye} - E_{NiO(100)}$). In the case of C343 the binding energies are close to ~-0.6/-0.7 eV (~-13/-16 kcal/mol); the CCO_2-B mode is slightly more stable than the CCO_2-M by ~0.12 eV. In CCO_2-M, the carbonyl oxygen is bound to one surface Ni atom and the carboxylic acid proton forms a

strong H-bond to one surface oxygen atom: the H atom is almost halfway the dye and the NiO oxygen atoms. In CCO_2-B, two bonds between the dye O atoms and the surface Ni are formed. These bonds also lead a structural distortion at the electrode surface where the Ni atoms move upward with respect to their minimum energy structure. Structural distortion from $O\text{-}H_{(dye)}$ and $Ni\text{-}O_{(NiO)}$ bond formation in each mode can be evaluated from the RMSD value in Table 1. Regarding the $-PO_3H_2$ anchoring group, it is more strongly bound to NiO(100) than $-CO_2H$: E_{ads} values are around ~-0.8/-1.0 eV (~-19/-23 kcal/mol). The three modes (M, B and T) are also very close in energy, they all lie within a ~0.15 eV window. CPO_3-B is the most stable, thanks to a favorable balance between formation of Ni-O bonds and surface distortion upon dye binding. Shorter $O\text{-}H_{(dye)}$ and longer $O\text{-}H_{(dye)}\cdots O_{NiO}$ bond lengths indicate that H bonding is weaker in CPO_3-M than in CCO_2-M. $O_{(dye)}$-Ni bond lengths are quite similar in all three cases. Overall, the largest surface distortion (RMSD) occurs for CPO_3-T, making it less convenient than CPO_3-B.

Since NiO electrodes in p-type DSSCs have a p-SC character, we have also considered absorption of CCO_2 and CPO_3 on p-type NiO(100). To model the electronic structure of a more realistic p-NiO electrode, we removed a neutral nickel atom from the central of the three bottommost layers in our slab, which correspond to introducing two holes into the total system. As expected, the main difference in the electronic structure of pristine NiO(100) and p-NiO(100) is the shift of the Fermi level well within the VB, as depicted by the atom- and angular-momentum projected density of states (PDOS) plots (see Figure S1 in electronic supporting information). All the qualitative features of NiO band edges are retained, with predominant VB and CB characters made of O *p* states and Ni *d* states, respectively (in agreement with recent studies on the same material).[25] We have calculated the p-NiO VB edge potential versus the Normal Hydrogen Electrode (NHE) and the open circuit potentials (V_{OC}) for clean p-NiO slab and all CCO_2/CPO_3-p-NiO(100) systems. Table 2 lists these relevant electronic features, as well as CCO_2/CPO_3binding energies in the different binding modes. E_{ads} values and their relative trend with respect of the binding modes are very similar to the case of pristine NiO(100), the most stable adsorption is still with the phosphonic acid group in the the CPO_3-B mode. Overall, differences in E_{ads} values between Ni(100) and p-NiO(100) are all within ~0.02 eV.

Open circuit potential (V_{OC}), an experimental observable, can be derived from the position of the p-NiO VB edge.[10] The V_{OC} is an important parameter to assess the DSSC performances, because it represents the upper limit of the possible electrical potential difference that can be delivered by the cell. Considering the I^-/I_3^- redox couple (0.354 V vs. NHE in acetonitrile),[26] we calculated V_{OC} as $V_{OC} = E_{I-/I3-} - E_{VB}$ (Scheme 1) for all CCO_2/CPO_3 binding modes (see Table 2). The p-NiO VB edge position and hence the V_{OC} are modified by the chemical nature of the anchoring group and by the different binding modes. Reported experimental values of V_{OC} for the CCO_2/p-NiO system in acetonitrile range from 70 to 117 mV.[27] Our computed V_{OC} values for CCO_2-M and CCO_2-B are 177 and 112 mV, respectively, which are qualitatively consistent with experimental data, considering that we are neglecting the solvent in our model. To the best of our knowledge, direct

experimental counterparts for the CPO_3/p-NiO V_{OC} are not available. However, a recent study on a p-type DSSC based on p-NiO and a metallo-organic dye with a phosphonic acid anchoring group[28] in acetonitrile reports a V_{OC} value of 95 mV, which is again of the same order of magnitude as our computed values. Overall, the V_{OC} of clean p-NiO(100) surface is always improved by the adsorption of the dye with a ΔV_{OC} from 11 to 76 mV.

A crucial parameter for efficient p-type DSSCs is also the energy difference between the dye HOMO and the p-NiO VB (ΔE in Scheme 1), which represents the thermodynamic driving force for the hole transport from the dye to the electrode. Defined in this way, ΔE should be large (and negative if defined as p-SC VB energy minus dye HOMO energy) in order to maximize the driving force for hole-injection and p-DSSC efficiency. Figure 3 depicts the atom- and angular moment- projected density of states (PDOS) for the two dye-electrode systems and their different possible binding modes. In all cases, the Fermi level crosses the Ni d- and O_{NiO} p- states (i.e., the p-NiO VB edge) that are higher in energy than dye HOMO energies. This means that ΔE values are all negative, which is favorable for having a convenient hole injection from the dye to the p-SC electrode. However, looking at the energy difference between the dye HOMOs and the corresponding Fermi level (Fig. 3c) we found that the nature of the binding group and the binding modes strongly affect the relative positions of HOMOs and VB edges and, thus, ΔE are not equally favorable in all the cases. ΔE value for CCO_2-B (-0.6 eV) is significantly lower than the CCO_2-M (-1.0 eV) one; the ΔE values for CPO_3-B and CPO_3-T (-0.17 and -0.10 eV, respectively) are much lower than the CPO_3-M ΔE value (-0.86 eV). The only binding mode that guarantees large (negative) ΔE value is the mono-dentate for both the Coumarin-based dyes under study.

We performed a detailed analysis of the electronic densities in order to dissect the origin of these differences in ΔE values: we found an inverse linear correlation between ΔE and the interfacial electrostatic dipole generated by the corresponding anchoring group/mode at the dye-electrode interface, as depicted by Figure 4. In particular, the dipole moment component along the direction perpendicular to the surface ($D_{Z,}$ calculated as described in Fig. 4b) has direct correlation to the energy difference value (ΔE). Thus, the observed ΔE trend is due to an electrostatic polarization by the dipole at the interface, which is responsible to shift up or down the dye HOMO energies. This interfacial dipole moment depends exclusively on the binding modes involving the anchoring groups and the p-NiO topmost atomic layer: nickel and oxygen atom displacements (outward the surface) because of Ni-$O_{(dye)}$ and O-$H_{(dye)}$ bonds are responsible for the observed interfacial dipole. The most favorable ΔE values for hole injection are those where the interfacial dipoles have the lowest absolute value. In other words, the hole-injection driving force has a maximum value when there is a minimum structural distortion at the p-NiO-dye interface. This is why CCO_2-M and CPO_3-M binding modes are the thermodynamically most convenient for ~~and efficient~~ hole injection. Our findings are consistent with and explain recent experimental observations that surface protonation of NiO decreases the driving force for dye-electrode hole injection.[29]

We must note that the overall efficiency of the hole injection process depends not only on the thermodynamic driving force, responsible for the irreversibility of the hole transfer, but also on the kinetic rates. The charge-transfer injection times depend on the dye-electrode interfacial properties, and, hence, on the binding groups/modes. In particular, theoretical studies on n-type DSSC model systems have shown that injection times are sensitive to the coupling term between the dye molecular orbitals and the semiconductor band states.[15] Several dyes featuring -CO_2H and -PO_3H_2 anchoring groups present faster injection times with the bidentate mode than with the monodentate one when adsorbed on TiO_2 anatase surfaces. In other words, on average, two direct dye-electrode bonds allow a faster charge transfer than one single bond. However, there are cases where the injection times are not sensitive to the binding modes (see for example Table 3 in Ref. 15h). This suggests that there are specific dyes that do not follow the general trend and that a careful analysis of kinetic features should be carried out on case-by-case basis. Moreover, these studies are based on the couplings between the dye LUMO and the n-SC conduction band, while in p-type DSSCs the hole injection involves dye HOMO and p-SC valence band. For these reasons, the knowledge of electron injection kinetics in n-type DSSCs cannot be straightforwardly applied to the hole-injection behavior in p-DSSCs. Ab initio calculations of injection times for different dyes and binding modes on p-NiO are also needed to obtain a complete picture of the hole injection process. Investigations on the hole transport kinetic features are beyond the purpose of this paper but are a subject of our ongoing work.

Overall, the possibility of control and select only ~~mono-dentate~~ the most convenient dye binding modes could boost the performances of p-type DSSC devices. From the perspective of computational screening of new anchoring groups, the interfacial electrostatic dipole formed upon dye adsorption represents a first useful descriptor to assess the quality of the anchoring group: those forming the lowest interfacial dipole are those with the highest potential for p-type DSSC.

Conclusions

In the present work we report a first-principles study on the structural and electronic features of the interfaces between two Coumarin-based dyes and the p-NiO(100) surface, two prototypical dye-electrode models of p-type DSSC devices.

We focused our attention on the effect of binding groups/modes on the electronic properties that are relevant for p-DSSC devices. We compared two anchoring groups: the most common carboxylic acid group and the recently proposed phosphonic acid. We investigated all the different possible binding modes on NiO(100) and p-NiO(100) and we found that both the chemical nature of the anchoring groups and the binding mode largely affect three important features of the dye-electrode interface: (1) the binding strength of the dye to the surface; (2) the open circuit potential V_{OC} values; and (3) the energy difference between dye HOMO and p-NiO VB edge (ΔE) as the driving force for dye-elctrode hole injection. Our results on dye-electrode anchoring strength show that the phosphonic acid group provides a stronger binding than

the carboxylic one by ~0.3 eV. The reason is the presence of an extra O atom / OH group able to interact with the surface; indeed, ~-0.3 eV is the average binding energy per O atom of the anchoring group. Energy differences among binding modes are small. The final E_{ads} trend derives from a balance between the convenient formation of Ni-$O_{(dye)}$ bonds and the inconvenient surface distortion effects.

Regarding the electronic properties at the dye-electrode interface, we focused on the more realistic p-type NiO(100) surface. Overall, we found good qualitative agreement between the computed V_{OC} values and their experimental counterparts, which confirms the adequacy of our model. Upon adsorption of the dye, the V_{OC} value increases with respect to the clean p-NiO surface for all the possible binding modes. However, upon dye adsorption we found very small shifts of the V_{OC} values (on the order of tens of meV) with no direct correlation with structural or electronic features of dye-electrode interfaces. The highest V_{OC} values (i.e., best for p-DSSC performance) correspond to the mono-dentate binding modes for both carboxylic acid and phosphonic acid anchoring groups.

We found a much more significant impact of the binding modes on the energy level alignments. In all the investigated cases, the energy of the dye HOMO lies below the p-NiO VB edge, i.e. pointing toward a favorable hole injection from the dye to the electrode. The absolute ΔE values depend strongly on the binding modes: the highest |ΔE| value (i.e., the strongest driving force for the hole injection) is obtained by mono-dentate binding for both CCO_2 and CPO_3.

The origin of the observed ΔE trend lies in an electrostatic polarization by the interfacial dipole moment along the direction perpendicular to the electrode surface. This dipole is determined by the binding mode and how it alters the structure of the topmost atomic layer of the electrode surface.

In summary, our analysis highlights that both the chemical nature of the anchoring group and the specific binding modes can significantly affect the electronic interfacial features that regulate performance in p-DSSCs. Our *ab initio* study suggests that synthetic strategies promoting selectively the mono-dentate binding mode for both carboxylic and phosphonic acid groups could significantly improve the thermodynamic driving force for hole injection in p-DSSCs based on a Coumarin dye. More generally, the choice of anchoring groups/binding modes that minimize the interfacial dipole moment could enhance the driving force for hole transport. Such information must be coupled with the knowledge of hole injection kinetics in order to choose the best performing systems for p-DSSCs. Further studies will investigate these kinetic features as well as the charge recombination process, which is also a main limiting process for current p-type DSSC. Proper modeling of these aspects would require the reliable description of the dye's electronic excited states, with methods beyond ground state DFT+U. From the present work, we are currently improving our model in the direction of including excited states and solvent medium, in order to extend further our fundamental understanding of p-type DSSC processes.

Computational details

In this work, we characterize the structural, energetic and electronic features of Coumarin-based dyes/NiO(100) interfaces by performing periodic spin-polarized density functional theory (DFT)+U[20] calculations with projector-augmented wave (PAW) potentials and plane wave basis set, as implemented in the VASP code (version 5.2.2).[30] The DFT+U approach has been proven to describe properly strongly correlated materials since it corrects the large self-interaction error (SIE) inherent in pure DFT when applied to localized electrons such as d-state in transition metal oxides.[31] We use the Perdew−Burke−Erzenhof (PBE)[32] exchange-correlation functional and the standard PAW potentials We use the *ab initio*-derived U-J value of 3.8 eV for describing the 3d states of Ni^{2+} ions, this U-J value has been validated in recent works on NiO.[25] A kinetic energy of 800 eV was used to converge the plane-wave basis set. We used a 4x4x1 k-point sampling based on the Monkhorst-Pack scheme for all calculations with the NiO slab described below. These parameters ensure a convergence on the total energy to within 1meV per formula unit.

Our model electrode is a 5-layer slab of a 2x2 unit cell of NiO (100) containing eight formula units per slab for a total of 80 atoms. This slab was generated by cleaving rocksalt NiO bulk structure with the theoretically determined lattice constant of a_{theo}=4.22 Å. This lattice constant is in agreement with recent similar *ab initio* studies[25] and 0.96% larger than the experimental value (a_{exp}=4.18 Å).[33] We set Ni spin-moments anti-ferromagnetically aligned along the (111) direction, as observed experimentally.[33] We have considered adsorption of one Coumarin-based dye per 2x2 NiO supercell, which corresponds to an almost full coverage, as desired in DSSC devices. The dye is adsorbed in only one side of the slab so dipole corrections have been always applied to avoid long-range polarization from the periodic images along the *z* direction.[34] We used a lattice constant of 40 Å for the *z* axis, which corresponds to a separation between periodic images of ~15 Å and prevents them from interacting.

The NiO(100) and dye/NiO(100) relaxed geometries were obtained by allowing the full relaxation of the atoms of both the two NiO uppermost layers and the attached dye (when present), keeping the three bulk-like bottommost layers fixed to mimic a semi-infinite bulk NiO crystal.

We computed the adsorption energies (E_{ads}) from $E_{ads} = E_{dye/NiO(100)} - E_{NiO(100)} - E_{dye}$, where $E_{dye/NiO(100)}$, $E_{NiO(100)}$ and E_{dye}, are the electronic energies of the relaxed dye/NiO(100), NiO(100) and isolated dye structures, respectively. Defined in this way, negative values of E_{bind} correspond to favored adsorption. E_{dye} has been obtained from periodic DFT-PBE calculations, where the dyes structures have been optimized in 18 Å x 18 Å x 18 Å unit cells. HOMO-LUMO plots of Fig. 1 have been obtained using the Gaussian09 code [35] at the DFT-PBE/6-311++G(2d,2p)[36] level of theory on the periodic DFT-PBE minimum energy geometry.

The p-type NiO slab model was obtained by removing a neutral Ni atom from the central of the three bottommost frozen layers of the pristine surface slab.

The NiO VB edge positions have been computed with DFT+U by considering the highest occupied Kohn-Sham eigenvalue properly referenced to the vacuum level, according to the Janak theorem.[37] This

procedure corresponds to the calculations of the work function for each dye-electrode slab model.[38] In supporting information (Figure S2) we report the plots of the plane-average electrostatic potential along the direction perpendicular to the slab for extracting the vacuum level. Due to the approximate nature of the Kohn-Sham density functional we must consider our computed VB maximum values only as qualitative results because they represent an upper limit of the true VB edge positions. More refined theoretical approaches to compute semi-conductor band edge positions are available,[39] but they go beyond the purposes of the present work.

Conversion of electronic energies (in eV) to potential values vs NHE (in V) has been carried out according to a standard procedure.[40] All the images of molecular and crystal structures and iso-surface plots were obtained with the VESTA program.[41]

Acknowledgments

The authors kindly acknowledge funding from the Italian Ministry of Research and University (MIUR) under grants FIRB Futuro in Ricerca (RBFR122HFZ) and PRIN (2012NB3KLK).

References

[1] B. Parida, S. Iniyan, R. Goic, *Renewable Sustainable Energy Rev.* 2011, **15**, 1625-1636.

[2] B. O'Regan, M. Grätzel, *Nature* 1991, **353**, 737

[3] M. Urbani , M. Grätzel , Md. K. Nazeeruddin T. Torres *Chem. Rev.* 2014, **114**, 12330-12396.

[4] (a) A. Hagfeldt, G. Boschloo, L. Sun, L. Kloo, H. Pettersson, *Chem. Rev.* 2010, **110**, 6595; (b) Z. Sun, J.H. Kim, T. Liao, Y. Zhao, F. Bijarbooneh, V. Malgras, S.X. Dou *CrystEngComm* 2012, **14**, 5472-5478; (c) Z. Sun, J.H. Kim, Y. Zhao, D. Attard, S.X. Dou *Chem. Comm.* 2013, **49**, 966-968.

[5] (a) M. M.Lee, J. Teuscher, T. Miyasaka, T. N. Murakami, H. J. Snaith, *Science* 2012, **338**, 643; (b) N.-G. Park, *J. Phys. Chem. Lett.* 2013, **4**, 2423-2429; (c) C. Grätzel, M. S. Zakeeruddin, *Mater. Today* 2013, **16**, 11.

[6] (a) J. He, H. Lindström, A. Hagfeldt, S.-E. Lindquist, *Sol. Energy Mater. Sol. Cells.* 2000, **62**, 265; (b) A. Nakasa, H. Usami, S. Sumikura, S. Hasegawa, T. Koyama, E. Suzuki, *Chem. Lett.* 2005, **34**, 500; (c) A. Nattestad, A. J. Mozer, M. K. R. Fischer, Y.-B. Cheng, A. Mishra, P. Bäuerle, U. Bach, *Nat. Mater.* 2010, **9**, 31-35.

[7] M. A. Green *Third Generation PhotoVoltaics: Advanced Solar Energy Conversion,* Springer-Verlag: Berlin, Heidelberg, 2003.

[8] F. Odobel, L. Le Pleux, Y. Pellegrin, E. Blart *Acc. Chem. Res.* 2010, **43**, 1063-1071

[9] F. Odobel, Y. Pellegrin, E. A. Gibson, A. Hagfeldt, A. L. Smeigh, L. Hammarström *Coord. Chem. Rev.* 2012, **256**, 2414-2423.

[10] S. Mori, S. Fukuda, S. Sumikura, Y. Takeda, Y. Tamaki, E. Suzuki, T. Abe *J. Phys. Chem. C* 2008, **112**, 16134.

[11] A. Morandeira, G. Boschloo, A. Hagfeldt, L. Hammarström, *J. Phys. Chem. C* 2008, **112**, 9530.

[12] A. Morandeira, J. Fortage, T. Edvinsson, L. Le Pleux, E. Blart, G. Boschloo, A. Hagfeldt, L. Hammarström, F. Odobel *J. Phys. Chem. C* 2008, **112**, 1721-1728.

[13] (a) F. Odobel, Y. Pellegrin *J. Phys. Chem. Lett.* 2013, **4**, 2551-2564; (b) M. Yu, G. Natu, Z. Ji, Y. Wu *J. Phys. Chem. Lett.* 2012, **3**, 1074

[14] E. A. Gibson, A. L. Smeigh, L. Le Pleux, J. Fortage, G. Boschloo, E. Blart, Y. Pellegrin, F. Odobel, A. Hagfeldt, L. Hammarström, *Angew. Chem. Int. Ed.* 2009, **48**, 4402.

[15] (a) F. De Angelis, S. Fantacci, A. Selloni, M. Graetzel, M. K. Nazeeruddin *Nano Lett.* 2007, **7**, 3189-3195; (b) Y. Bai, I. Mora-Seró, F. De Angelis, J. Bisquert, P. Wang *Chem. Rev.* 2014, **114**, 10095-10130; (c) F. Ambrosio, N. Martsinovich, A. Troisi *J. Phys. Chem. Lett*. 2012, **3**, 1531; (d) N. Martsinovich, F. Ambrosio, A. Troisi *Phys. Chem. Chem. Phys*., 2012, **14**, 16668-16676; (e) F. Labat, T. Le Bahers, I. Ciofini, C. Adamo *Acc. Chem. Res.* 2012, **45**, 1268-1277; (f) T. Le Bahers, T. Pauporté, P. P. Lainé, F. Labat, C. Adamo, I. Ciofini *J. Phys, Chem. Lett.* 2013, **4**, 1044-1050; (g) N. Martisinovich, A. Troisi *Energy Environ. Sci.*, 2011, **4**, 4473; (h) F. Ambrosio, N. Martsinovich, A. Troisi *J. Phys. Chem. C* 2012, **116**, 2622–2629.

[16] (a) J. Preat, D. Jacquemin, E. A. Perpete *Energy Environ. Sci.* 2010,**3**, 891-904 (b) M. Gennari, F. Legalite, L. Zhang, Y. Pellegrin, E. Blart, J. Fortage, A. M. Brown, A. Deronzier, M. N. Collomb, M. Boujtita, D. Jacquemin, L. Hammarström, F. Odobel *J. Phys. Chem. Lett.* 2014, **5**, 2254-2258 (c) D. Jacquemin, E. A. Perpete, I. Ciofini, C. Adamo *Acc. Chem. Res.* 2008, **42**, 326.

[17] F. Trani, J. Vidal, S. Botti, M. A. L. Marques *Phys. Rev. B* 2010, **82**, 085115

[18] A. Morandeira, G. Boschloo, A. Hagfeldt, L. Hammarström *J. Phys. Chem. B* 2005, **109**, 19403.

[19] W. Kohn, L. J. Sham *Phys. Rev.* 1965, **140**, A1133-A1138

[20] (a) V. I. Anisimov, J. Zaanen, O. K. Anderson *Phys. Rev. B* 1991, **44**, 943; (b) V. I. Anisimov, I. V. Solovyev, M. A. Korotin, M. T. Czyżyk, G. A. Sawatzky *Phys. Rev. B* 1993, **48**, 16929; (c) N. J. Mosey, P. Liao, E. A. Carter, *J. Chem. Phys.* 2008, **129**, 014103.

[21] (a) A. Fujimori, F. Minami, Phys. Rev. B 1984, 30, 957-971; (b) S. Hüfner, *Adv. Phys.* 1994, **43**, 183-356; (c) I. de P. R. Moreira, F. Illas, R. L. Martin Phys. Rev. B 2002, **65**, 155102.

[22] J. Warnan, Y. Pellegrin, E. Blart, L. Zhang, A. Brown, L. Hammarström, D. Jacquemin, F. Odobel *Dyes and Pigments* 2014, **105**, 174-179.

[23] J. Cui, J. Lu, X. Xu, K. Cao, Z. Wang, G. Alemu, H. Yuang, Y. Shen, J. Xu, Y. Cheng, M. Wang *J. Phys. Chem. C* 2014, **118**, 16433.

[24] (a) J. M. Gardner, M. Beyler, M. Karnahl , S. Tschierlei , S. Ott , L. Hammarström *J. Am. Chem. Soc.* 2012, **134**, 19189; (b) M. Bräutigam, M. Schulz, J. Inglis, J. Popp, J. G. Vos, B. Dietzek *Phys. Chem. Chem. Phys.* 2012, **14**, 15185; (c) W. Hamd, M. Chavarot-Kerlidou, J. Fize, G. Muller, A. Leyris, M. Matheron, E. Courtin, M. Fontecave, C. Sanchez, V. Artero, C. Laberty-Robert *J. Mater. Chem. A* 2013,**1**, 8217.

[25] (a) N. Alidoust, M. C. Toroker, J. A. Keith, E. A. Carter *ChemSusChem* 2014, **7**, 195; (b) N. Alidoust, M. C. Toroker, E. A. Carter *J. Phys. Chem. B*, 2014, **118**, 7963-7971.

[26] G. Boschloo, A. Hagfeldt *Acc. Chem. Res.* 2009, **42**, 1819

[27] (a) A. Nattestad, M. Ferguson, R. Kerr, Y.-B. Cheng, U. Bach *Nanotechnology* 2008, **19**, 295304; (b) P. Qin, H. Zhu, T. Edvinsson, G. Boschloo, A. Hagfeldt, L. Sun *J. Am. Chem. Soc.* 2008, **130**, 8570-8571; (c) Y. Mizoguchi, S. Fujihara *Electrochem. Solid-State Lett.* 2008, **11**, K78-K80; (d) L. Lepleux, B. Chavillon, Y. Pellegrin, E. Blart, L. Cario, S. Jobic, F. Odobel *Inorg. Chem.* 2009, **48**, 8245-8250.

[28] Y. Pellegrin, L. Le Pleux, E. Blart, A. Renaud, B. Chavillon, N. Szuwarski, M. Boujtita, L. Cario, S. Jobic, D. Jacquemin, F. Odobel *J. Photochem. Photobiol. A* 2011, **219**, 235-242

[29] J. Cui, J. Lu, X. Xu, K. Cao, Z. Wang, G. Alemu, H. Yuang, Y. Shen, J. Xu, Y. Cheng, M. Wang, *J. Phys. Chem. C* 2014, **118**,16433-16440

[30] (a) G. Kresse, J. Furthmüller, *J. Comput. Mater. Sci.* 1996, **6**, 15; (b) G. Kresse, J. Furthmüller *Phys. Rev. B* 1996, **54**, 11169.

[31] (a) E. A. Carter, *Science* 2008, **321**, 800; (b) A. B. Muñoz-García, A. M. Ritzmann, M. Pavone, J. A. Keith, E. A. Carter Acc. Chem. Res. 2014, **47**, 3340.

[32] J. P. Perdew, K. Burke, M. Ernzerhof, *Phys. Rev. Lett.* 1996, **77**, 3865.[33] (a) F. Fiévet, P. Germi, F. De Bergevin, M. Figlarz, *J. Appl. Crystallogr.* 1979, **12**, 387; (b) L. C. Bartel, B. Morosin, *Phys. Rev. B* 1971, **3**, 1039; (b) R. J. Powell, W. E. Spicer, *Phys. Rev. B* 1970, *2*, 2182; (c)

[34] J. Neugebauer, M. Scheffler *Phys. Rev. B* 1992, **46**, 16967.

[35] Gaussian 09, Revision D.01, M. J. Frisch, G. W. Trucks, H. B. Schlegel, G. E. Scuseria, M. A. Robb, J. R. Cheeseman, G. Scalmani, V. Barone, B. Mennucci, G. A. Petersson, H. Nakatsuji, M. Caricato, X. Li, H. P. Hratchian, A. F. Izmaylov, J. Bloino, G. Zheng, J. L. Sonnenberg, M. Hada, M. Ehara, K. Toyota, R. Fukuda, J. Hasegawa, M. Ishida, T. Nakajima, Y. Honda, O. Kitao, H. Nakai, T. Vreven, J. A. Montgomery, Jr., J. E. Peralta, F. Ogliaro, M. Bearpark, J. J. Heyd, E. Brothers, K. N. Kudin, V. N. Staroverov, R. Kobayashi, J. Normand, K. Raghavachari, A. Rendell, J. C. Burant, S. S. Iyengar, J. Tomasi, M. Cossi, N. Rega, J. M. Millam, M. Klene, J. E. Knox, J. B. Cross, V. Bakken, C. Adamo, J. Jaramillo, R. Gomperts, R. E. Stratmann, O. Yazyev, A. J. Austin, R. Cammi, C. Pomelli, J. W. Ochterski, R. L. Martin, K. Morokuma, V. G. Zakrzewski, G. A. Voth, P. Salvador, J. J. Dannenberg, S. Dapprich, A. D. Daniels, Ö. Farkas, J. B. Foresman, J. V. Ortiz, J. Cioslowski, D. J. Fox, Gaussian, Inc., Wallingford CT, 2009.

[36] M. J. Frisch, J. A. Pople, J. S. Binkley *J. Chem. Phys.* 1984, **80**, 3265

[37] J. F. Janak, Phys. Rev. B, 1978, 18, 7165.

[38] (a) G. Heimel, L. Romaner, E. Zojer, J.-L. Bredas, *Acc. Chem. Res.* 2008, **41**, 721-729; (b) H. Li, P. Winget, J.-L. Bredas *Chem. Mater.* 2014, **26**, 631-646 (c) G. F. Arnaud, V. De Renzi, U. del Pennino, R. Biagi, V. Corradini, A. Calzolari, A. Ruini, A. Catellani *J. Phys. Chem. C* 2014, **118**, 3910-3917

[39] M. C. Toroker, D. K. Kanan, N. Alidoust, L. Y. Isseroff, P. Liao, E. A. Carter *Phys. Chem. Chem. Phys.* 2011, **13**, 16644-16654

[40] Absolute energies in eV have been converted in potential values in V vs NHE according to the equation: {E(in V vs NHE) = -4.5 - E(in eV)}, from: *Handbook of electrochemistry.* Ed.: C. G. Zoski, Elsevier, 2007

[41] K. Momma, F. Izumi *J. Appl. Crystallogr.* 2011, **44**, 1272-1276.

Table 1. Calculated adsorption energies and selected structural features of CCO_2 and CPO_3 dyes adsorbed on on NiO(100) surface in their different anchoring modes: mono-dentate (M), bi-dentate (B) and tri-dentate (T): distances between O atoms of the anchoring group and surface Ni ($d(O_{(dye)} – Ni)$); O-H bond lengths in the undissociated carboxylic and phosphonic groups ($d(O\text{-}H_{(dye)})$); hydrogen bond length between the undissoaciated OH groups and surface O ($d(O\text{-}H_{(dye)} \cdots O_{(NiO)})$); O-H bond lengths in the hydroxyl group created upon dissociation in the bidentate and tridentate modes ($d(O\text{-}H_{(dye)})$); displacements along z axis with respect to clean surface positions (Δz) of surface Ni and O atoms bonded with the dye or bearing an H and root mean square deviation (RMSD) of the topmost NiO(100) atomic layer.

	CCO_2-M	**CCO_2-B**	**CPO_3-M**	**CPO_3-B**	**CPO_3-T**
E_{ads} (meV)	-591	-708	-841	-998	-886
$d(O_{(dye)} – Ni)$ (Å)	2.024	2.027 2.008	2.048	2.012 2.011	2.058 2.016 1.979
$d(O\text{-}H_{(dye)})$ (Å)	1.184	-	1.053 1.034	0.985	-
$d(O\text{-}H_{(dye)} \cdots O_{(NiO)})$ (Å)	1.265	-	1.530 1.617	2.104	-
$O\text{-}H_{(NiO)}$ (Å)	-	0.981	-	0.987	1.003 0.987
Δz_{Ni} (Å)	0.133	0.171 0.177	0.139	0.143 0.178	0.018 0.232 0.296
Δz_O (Å)	0.132	0.380	0.094 0.093	0.358 0.000	0.320 0.271
RMSD (Å)	0.052	0.146	0.080	0.129	0.177

Table 2. Calculated adsorption energies of CCO_2 and CPO_3 dyes on p-type NiO(100) (E_{ads}) and electronic features of the corresponding model p-DSSC devices: p-NiO valence band (VB) edge position (V vs NHE) and open circuit voltage (V_{OC}) values (vs I^-/I_3^- redox couple at 0.354 V vs NHE, see **Scheme 1**).[26] V_{OC} experimental values are reported in parentheses.

	p-NiO	**CCO_2-M**	**CCO_2-B**	**CPO_3-M**	**CPO_3-B**	**CPO_3-T**
E_{ads} (meV)	-	-581	-722	-806	-999	-909
p-NiO VB (V)	0.455	0.531	0.466	0.481	0.482	0.466
V_{OC} (mV)	101	177 (76-116)[a]	112	127	128 (95)[b]	112

(a) Ref. 27; (b) Ref. 28.

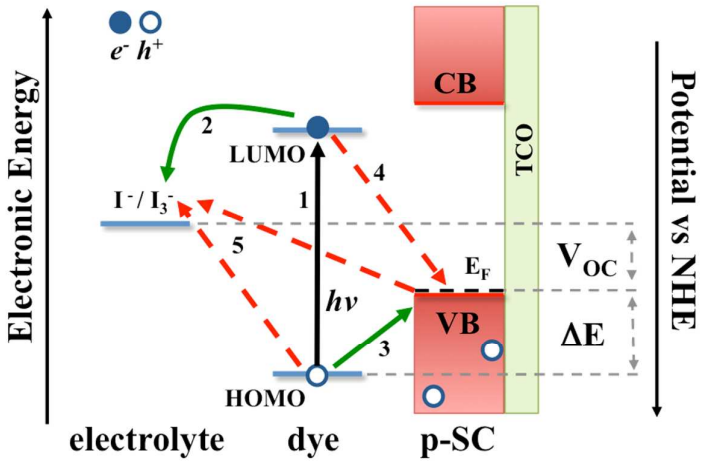

Scheme 1. Scheme of Functioning of a photocathode in p-type DSSC: (1) excitation of the dye; (2) electron injection from the excited dye to the electrolyte; (3) electron injection from the p-type SC valence band (VB) to the dye HOMO; (4) charge recombination at the dye p-SC interface and (5) hole injection from the dye (or from the p-SC VB) to the electrolyte. Green solid arrows represent desired electron/hole injection, dashed red lines show undesired recombination processes.

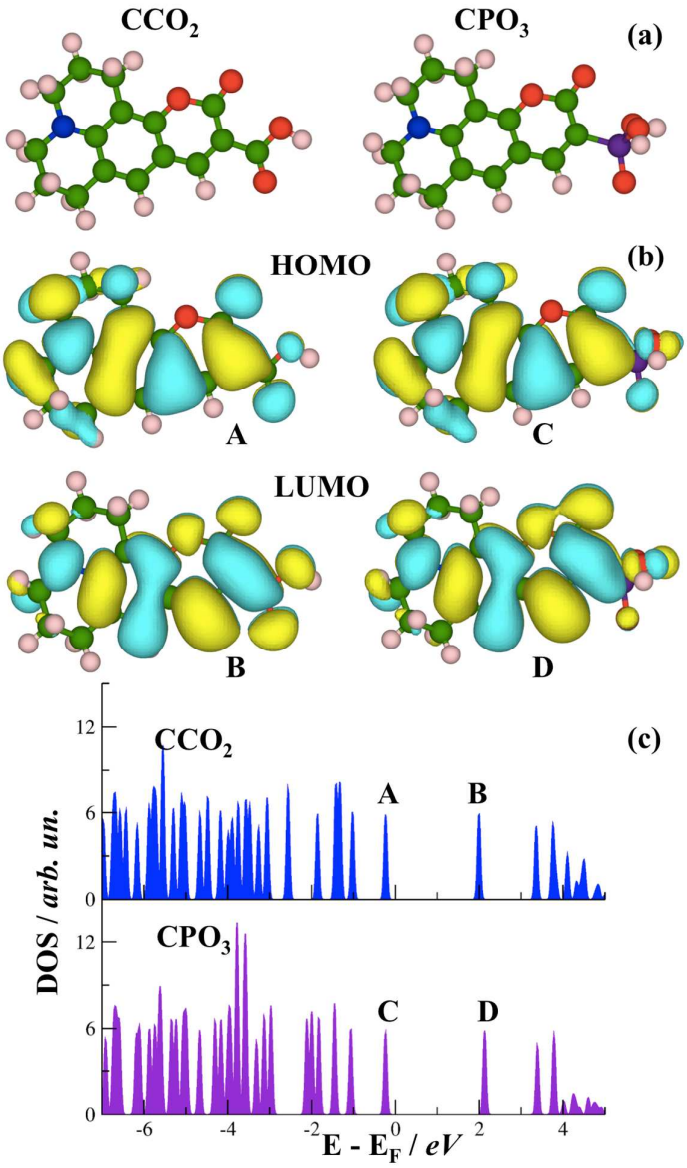

Figure 1. (a) Optimized structures of the two isolated Coumarin-based dyes under study: C343 (CCO_2) and C6H-PO_3H_2 (CPO_3) (b) highest occupied molecular orbitals (HOMO) and lowest unoccupied molecular orbitals (LUMO) orbitals of CCO_2 and CPO_3, computed at the DFT-PBE/6-311++G(2d,2p) level of theory. (c) Total density of states (DOS) of CCO_2 and CPO_3 with periodic DFT-PBE level of theory, the Fermi energy is set to zero. Color legend: C (green); N (blue); O (red) and H (light pink).

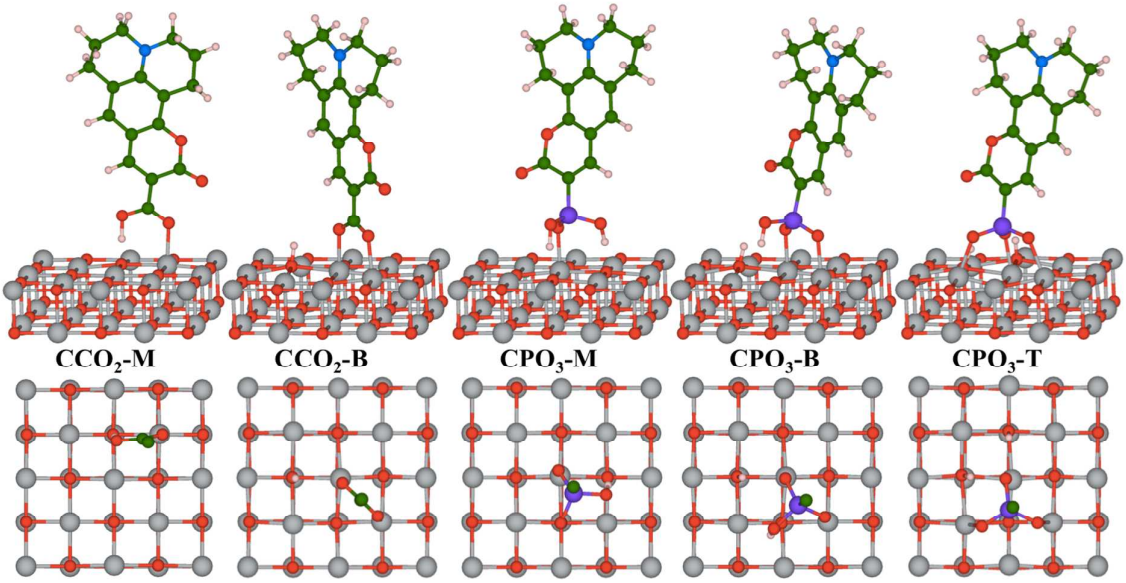

Figure 2. (Top) Optimized structures of the adsorbed CCO_2 and CPO_3 dyes upon adsorption on NiO(100) in the monodentate (M), bidentate (B) and tridentate (T) modes. Lateral view. For clarity, only the two topmost NiO atomic layers are displayed. (Bottom): Top view of the same structures showing only the COOH and PO_3H_2 anchoring groups. Color legend: C (green); N (blue); O (red) and H (light pink), Ni (grey), P(violet).

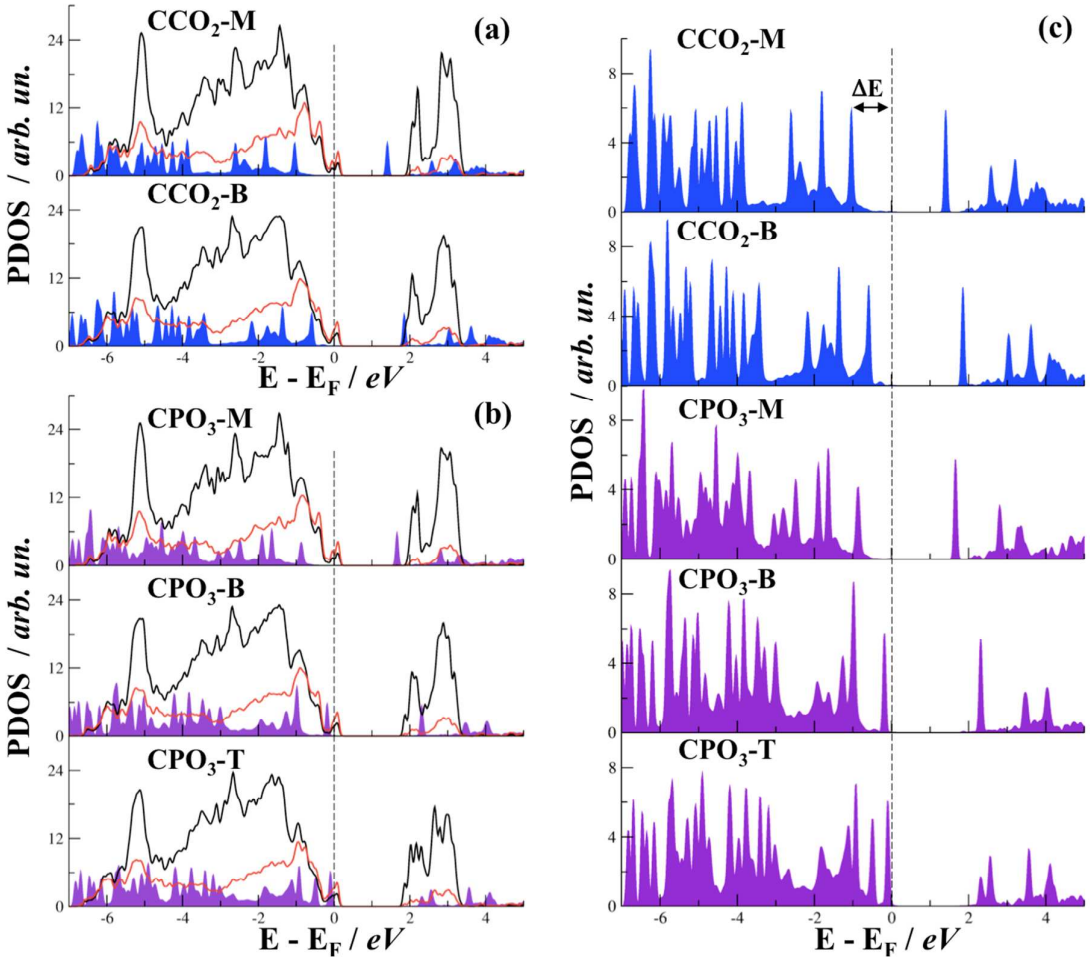

Figure 3. (a) projected density of states (PDOS) of Ni (black line), O(red line) and dye (solid blue pattern) for CCO_2-M and CCO_2-B (b) projected density of states (PDOS) of Ni (black line), O(red line) and dye (solid violet pattern) for CPO_3-M, CPO_3-B and CPO_3-T. The Fermi energy (E_F) is set to zero. (b) Zoom-in near the Fermi level. For clarity, only PDOS of the dye are shown. ΔE values are reported in the main text, they are calculated as the energy difference between the Fermi level (p-NiO VB edge) and the dye highest occupied PDOS peak.

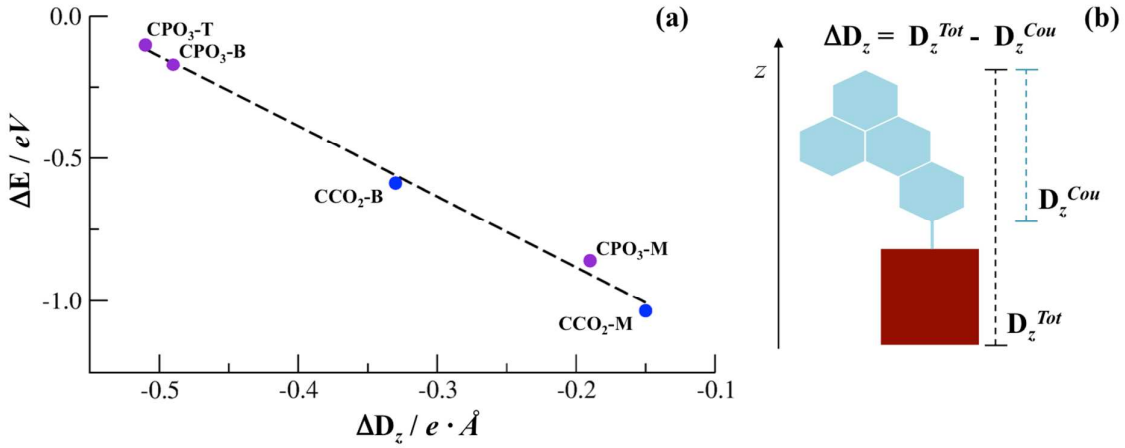

Figure 4. (a) ΔE (energy difference between dye HOMO and p-NiO VB edge) as a function of the interfacial electrostatic dipole along z axis (ΔD_z) for CCO_2-M, CCO_2-B, CPO_3-M, CPO_3-B and CPO_3-T systems (b) Schematic representation of ΔD_z, as calculated from the total dipole (ΔD_z^{Tot}) and the dye dipole (ΔD_z^{Cou}) along the z axis.